DOI: 10.21062/mft.2026.034 http://www.journalmt.com

Impact of Infill Patterns and Densities on the Mechanical Strength of FDM 3D-Printed Components

Marija Dimovska (0009-0007-0224-0680), Nenad Radenkovikj (0009-0003-8666-2805), Ognen Tuteski (0000-0002-0379-0031), Ema Vasileska (0000-0003-3937-0546), Boban Kusigerski (0009-0003-4788-4579), Mite Tomov (0000-0002-4386-7419), Valentina Gechevska (0000-0001-9353-6899)
Faculty of Mechanical Engineering - Skopje, Ss. Cyril and Methodius University in Skopje, Ruger Boskovic 18, 1000 Skopje, R. Macedonia. E-mail: ognen.tuteski@mf.edu.mk

Additive manufacturing (AM), more commonly known as 3D printing, is a highly convenient manufacturing process that enables the creation of complex 3D objects. The large body of literature proved that the choice of material, the printing technology used, and the values of certain process parameters all influence the mechanical behavior of the final part. In this study, the Fused Deposition Modeling (FDM) technology was used to manufacture standardized test specimens, which were all subjected to mechanical testing. The main aim of the research was to investigate the effects of various infill patterns, combined with various infill densities, on tensile strength, and thus determine the patterns that enhance better structural performance. Three infill density levels were analyzed along with five infill patterns. A systematic sequence of tensile tests traced the correlation between internal material distribution and measured mechanical properties. By systematically varying the infill parameters, this study provides valuable insights into selecting appropriate configurations for specific applications. The findings contribute to advancements in AM design and material utilization, leading to stronger and more efficient components.

Keywords: FDM technology, 3D printing, Tensile strength, Infill patterns, Infill density

1 Introduction

FDM is one of the most popular 3D printing technologies due to its versatility, affordability, and the ability to create complex shapes. Materials commonly used include PLA, ABS, PETG, TPU, and Nylon, each offering unique properties like strength, flexibility, or heat resistance [1,2,3]. Among these, PLA (Polylactic Acid) stands out as an eco-friendly, easily available material that can be sourced using renewable sources [4]. Its low warping tendency, wide variety of color availability, and overall high-quality surface finish make PLA especially well-suited to prototyping, cosmetic parts, and education. This study focuses exclusively on PLA plastic due to its relative accessibility and ease of use [2].

The performance of FDM-printed components is affected by a large number of variables such as printing temperature [5], layer height, humidity, material and print speed [3,6]. Among them, the choice of infill pattern and density stand out as one of the most important parameters, which has a direct impact on the mechanical strength, material efficiency, and structural integrity [7,8,9,10]. This study will therefore focus on these two parameters, as they are among the most controllable and impactful aspects of the printing process.

2 Literature review

Recent developments in AM have led to an extensive research of the influence of the infill parameters, i.e., pattern, density, and layer thickness, on the mechanical behavior of 3D printed components. The large body of empirical findings supports the assumption that these parameters have a determinant effect on tensile, compressive, and flexural and impact strength, which depends on the material composition and specific application demands.

Agrawal et al. [3] investigated the interaction between infill pattern, infill density, and layer thickness in ABS compo-nents manufactured using FDM. They found that concentric infill of 80 % density and 100 μm layer thickness produced better tensile and impact strength as compared to line and triangle infill. Similarly, Rismalia et al. [4] validated the effectiveness of concentric infill to improve tensile strength in PLA, especially at higher infill densities, which demonstrated a strong relationship between pattern choice and mechanical properties.

Being limited to PLA, PLA+, and PETG, Kadhum et al. [8] compared fourteen infill patterns in detail. They demonstrated the advantages of cubic, gyroid and concentric infill in terms of mechanical strength,

and cross infill and quarter-cubic infill in terms of surface quality. This analysis can therefore explain the nuanced balance between strength and finish in material-specific scenarios.

Liu et al. [1] studied carbon-fibre-reinforced nylon and showed that at same mass, triangular infill had the maximum compressive strength compared to gyroid and rectangular shapes. The triangular infill of 41 % was considered to provide the best balance between weight and strength, which is of special interest to prosthetic use. In a parallel study on carbon fiber-reinforced PETG, Patil et al. [2] discovered that compressive strength increased with higher infill densities, with the tri-hexagon pattern at 80% yielding a peak value of 39.16 MPa. Their usage of response-surface methodology also enabled predictive modelling of mechanical behaviour at different conditions.

These findings have been extended by Karad et al. [6] on ABS materials and have shown that the tensile and flexural outcomes were directly correlated with the infill density, especially in the line and triangular patterns. The results of scanning electron microscopy indicated that denser infills results in higher microstructural integrity through a reduction in porosity and fracture of the matrix. Birosz and Ando [7] also point at the possibility of reducing print time without affecting stiffness in PLA specimens by means of infill-pattern scaling and, thus, demonstrating new ways of optimizing efficiency in FDM.

In Joska et al. [11] the authors examined the influence of the shape and density of infill on the mechanical properties of 3D-printed PLA specimens, using honeycomb and gyroid patterns at varying infill densities. Findings in the tensile testing revealed that infill geometry only had a minor impact on absolute tensile strength however gyroid shapes showed a slight, but pronounced, benefit over honeycomb at higher density values. Analysis also showed that gyroid filled designs were more efficient in terms of saving average print time as compared to honeycombs by 23.73 %. Lastly, the surface hardness of the specimens was found to vary based on the print orientation with the surface touching the print showing a 13.6 % increase in hardness. The fractographic analysis showed that infill type had insignificant influence on fracture morphology at low densities, but significant differences were observed at high densities: at high density, gyroid patterns were observed to enhance predominantly transverse fracture, whereas honeycomb patterns enhanced angled fracture.

Previously conducted theoretical research (e.g., [3,6,7,8]) determines that the grid and gyroid patterns are among the infill schemes that have favourable mechanical performance. However, the relationship between infill pattern and density is still rather under-researched. Based on these studies, infill strategy is a critical element in the determination of the mechanical properties of 3D-printed parts. The most beneficial designs are always the concentric and triangular ones when the strength-based requirements prevail. Additional increases in structural performance are achieved with a scale of methodologies or reinforcement fibres like carbon fibres.

This study is an attempt to fill this knowledge gap with a systematic assessment in order to find the infill pattern that provides the most beneficial trade off between the mechanical performance and material efficiency. The insights derived are valuable in guiding optimisation of FDM processes and in improving the mechanical properties of 3D printed components in engineering, prototyping and manufacturing.

3 Materials and methods

3.1 Printing Setup

For the experiment, a generic PLA brand was used. PLA is a biodegradable thermoplastic with excellent printability, low shrinkage, and strong interlayer adhesion, making it suitable for detailed and durable prints. This type of thermoplastic filament is one of the most frequently used raw materials in FDM printing due to its favorable printing behavior. The size of the printed standard specimens for tensile strength tests follows the ISO 527 standard for a 1A type dogbone shape (Fig. 3). The samples were printed on an Ender 3 V2 (Fig. 1), a reliable and widely used FDM printer. The G-Code preparation was done in the slicer Cura 5.9.0.

Although PLA is generally easy to print, its hygroscopic nature means that it can absorb moisture from the environment, which may influence print quality and mechanical properties. In this study, the filament was stored under standard laboratory conditions, but no active pre-drying procedure (such as heated drying or storage in a dry box) was performed. This introduces a potential source of variation, as moisture-laden PLA can exhibit increased porosity, micro-void formation, and reduced interlayer adhesion during extrusion. While all specimens were printed under identical conditions to maintain experimental consistency, the absence of moisture conditioning should be acknowledged as a factor that may affect the resulting tensile strength and ductility values.

Additionally, all specimens were printed in a single orientation, lying flat on the build plate with their

longitudinal axis aligned along the X–Y plane. This ensured uniformity across the experimental matrix but inherently reflects only one possible orientation in FDM processes. Since print orientation strongly influences interlayer bonding and final mechanical behavior, the results reported here represent this specific printing direction and do not encompass the full anisotropic nature of FDM-printed PLA.

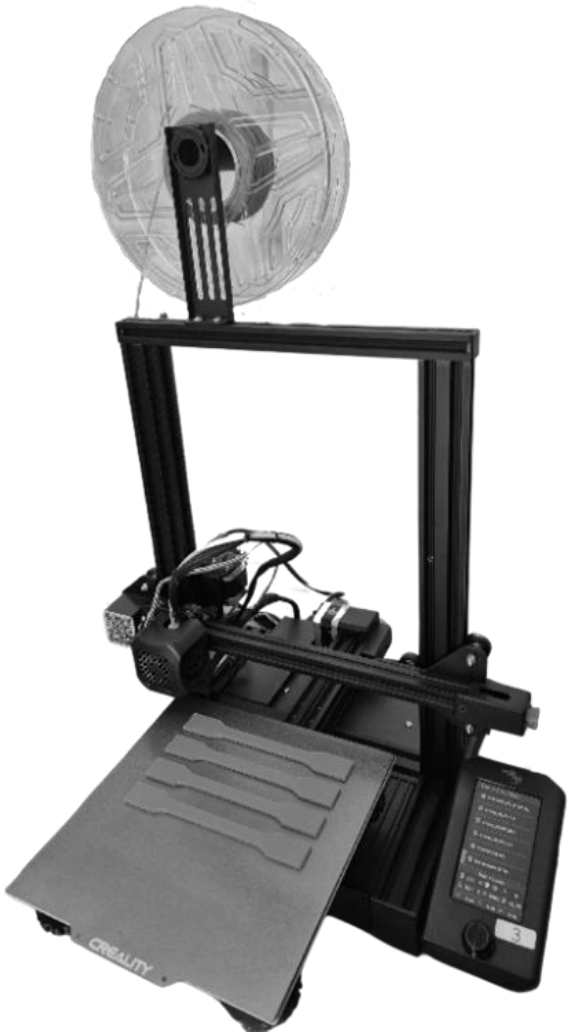

Fig. 1 *Creality Ender 3 V2*

3.2 Measurement Setup

The tensile test was done on a Shimatzu Autograph AGS-X machine, with a maximum load capacity of 10 kN. The test followed the ISO 527–2 standard procedure with a crosshead testing speed of 5 mm/min.

The tensile tests were conducted in accordance with ISO 527-1 standard (Fig. 3), where the force-displacement data generated during testing were captured and displayed through the connected computer interface. The produced specimens provide a visual basis for comparing their influence on mechanical properties (Fig. 4). The results were evaluated using the TRAPEZIUMX software used to operate and control the Shimadzu AGS-X testing machine.

There were 45 specimens that were analyzed, and it was ensured that the specimen was placed properly between the grips of the machine to eliminate inaccurate alignment. Prior testing, the force of the machine was adjusted to zero to provide a reference point of accurate measurement. Testing was started under a controlled parameter where the specimen was applied to uniaxial tensile load until failure of the specimen occurred. The identified expected breaking points were clearly marked on each specimen and allowed easy identification of fracture locations (Fig. 4). The machine provided detailed stress-strain data on every test and these data were recorded and stored systematically.

Fig. 2 *Shimadzu Autograph AGS-X 10kN*

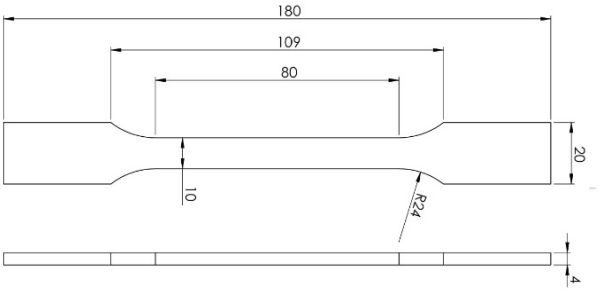

Fig. 3 *Specimen type 1A dimension in accordance with ISO 527-2 [12]*

Fig. 4 *Specimens after tensile testing*

3.3 Experimental Design

The experimental plan of this study was to determine the tensile strength of PLA (Polylactic Acid) specimens that were printed through Fused Deposition Modeling (FDM) 3D printing [13]. The main aim was to analyze the effect of the two fundamental parameters, the infill pattern and the infill density [14], on the mechanical properties of the parts. This was to be done by using five infill patterns (Fig. 5) and three infill densities (25%, 50%, and 75%) and resulted in a total of 15 unique combinations (Tab. 1). To ensure statistical reliability, three replicates were produced for each combination to obtain 45 specimens for testing.

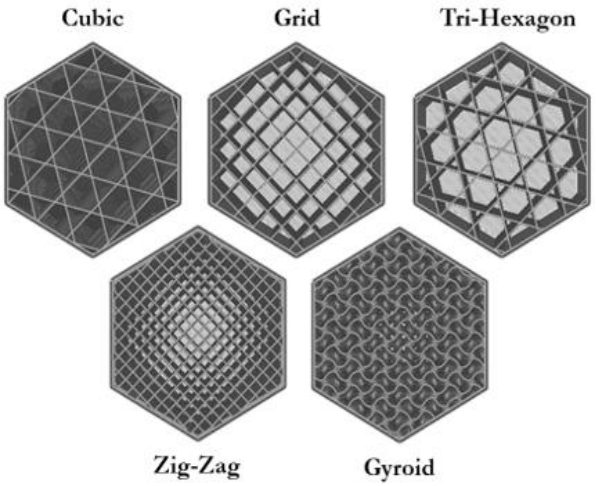

Numbering	Infill pattern
1	Cubic
2	Gyroid
3	Tri - Hexagon
4	Zig - Zag
5	Grid

Fig. 5 *Infill patterns*

Tab. 1 *Experiment design matrix*

Combination no.	Variable factors	
	Infill pattern [-]	Infill density [%]
1	Cubic	25
2	Cubic	50
3	Cubic	75
4	Gyroid	25
5	Gyroid	50
6	Gyroid	75
7	Tri - Hexagon	25
8	Tri - Hexagon	50
9	Tri - Hexagon	75
10	Zig - Zag	25
11	Zig - Zag	50
12	Zig - Zag	75
13	Grid	25
14	Grid	50
15	Grid	75

The rest of the process parameters, i.e., layer height, nozzle temperature, print speed were maintained the same in all experimental conditions (Tab. 2), thus isolating the effects of infill pattern and density on mechanical performance.

Tab. 2 *Fixed and variable factors in the experiments*

Fixed Parameters	**Values**
Nozzle diameter	0.4 mm
Layer height	0.2 mm
Wall thickness	0.8 mm
Top/Bottom layers	4 layers
Nozzle temperature	200 °C
Build plate temperature	60 °C
Printing Speed	50 mm/s
Variable factors	**Values**
Infill density	25%; 50%; 75%;
Infill pattern	Cubic; Gyroid; Tri Hexagon; ZigZag; Grid;

4 Results and Analysis

This section presents the results obtained from the experiments and provides an analysis to address the research objectives. The results in the form of σ-ε stress strain curves are graphically plotted on Fig. 6, grouped according to the specimen infll density. The three stress–strain graphs depict the mechanical behavior of different infill patterns, Cubic, Grid, Gyroid, TriHexagon, and ZigZag, at infill densities of 25%, 50%, and 75%.

As we can see from the provided σ-ε curves, the PLA material that was tested was quite brittle with all specimens across the 3 infill desities and 5 infill patterns showing little to no plastic deformation before the break point.

- At 25% infill, the specimens from all patterns display similar initial elastic behavior, but the ZigZag infill has the highest peak stress and strain, indicating better overall ductility and strength. The Grid and TriHexagon patterns have slightly lower ultimate stress values, suggesting less efficient load distribution at this low density.
- At 50% infill, the differences between patterns become more pronounced. The patterns Gyroid and ZigZag reach higher ultimate stresses and sustain larger strains before failure, indicating a more favorable balance between strength and deformability. The TriHexagon infill, in contrast, reaches peak stress earlier and exhibits a shorter strain range, suggesting reduced ductility.
- At 75% infill, again the Gyroid pattern achieves the highest ultimate stress, with ZigZag following closely behind in strength. Here the TriHexagon shows a more brittle behavior. These curves confirm that as infill density increases, all patterns improve in strength, but the relative efficiency of each pattern also becomes more distinct.

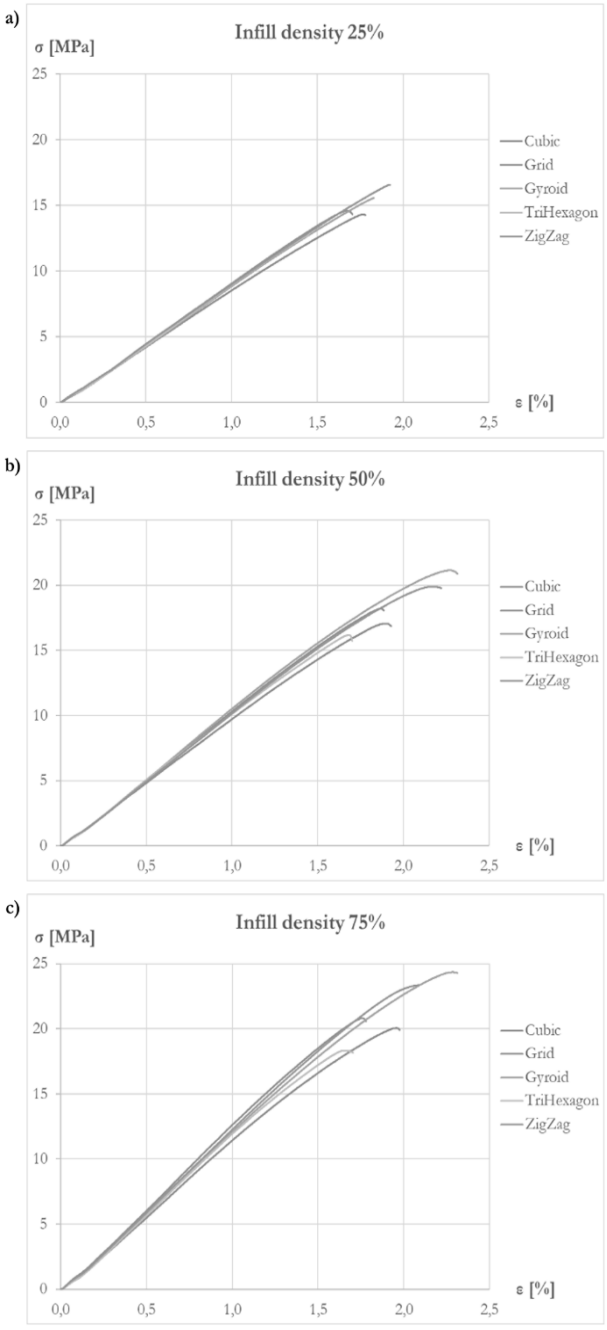

Fig. 6 *Stress-strain curves for all tested infill patterns; a) 25% infill density; b) 50% infill density; c) 75% infill density*

The additional ANOVA study of the experimental data was conducted using Minitab software and determined that there is a significant dependency between the infill pattern and infill density. To gain a deeper understanding, three separate analyses were performed for each response. The first analysis focused on tensile strength (σ), examining how changes in infill pattern and infill density impact the material's ability to withstand tension. The second analysis investigated strain (ε), evaluating the standard deviation and variability of the responses to determine the consistency of the material's behavior under different conditions. Lastly, the third analysis concentrated on the modulus of elasticity (E), measuring the material's stiffness and its ability to deform elastically under applied stress. Regresional models were developed that provide insights into how the infill pattern and density contribute to the mechanical properties of the material, offering valuable data for optimizing design and manufacturing processes.

4.1 Decoding a discrete variable into substitute numerical variables

Since the Infill pattern, as a variable factor is a discrete (categorical) variable, in order to include it into the regression models we need to decode it into substitute variables (dummy variables). This way it's possible to include the information from the different infill patterns into the regression model. This is necessary because regression models operate exclusively with numerical variables.

Through this mathematical transformation of decoding, the categorical information is transformed into a form that can be included in the regression model and used to analyze the impact of the different values of the categorical variable on the dependent variable. For each data entry, the corresponding dummy variable is set to 1 if the entry matches that value, or to 0 if it does not. For example, if the infill pattern is Cubic, then the corresponding dummy variable for Cubic will be equal to 1, while the other four, Gyroid, Tri – Hexagon, Zig – Zag and Grid, will be equal to 0 (Tab. 3).

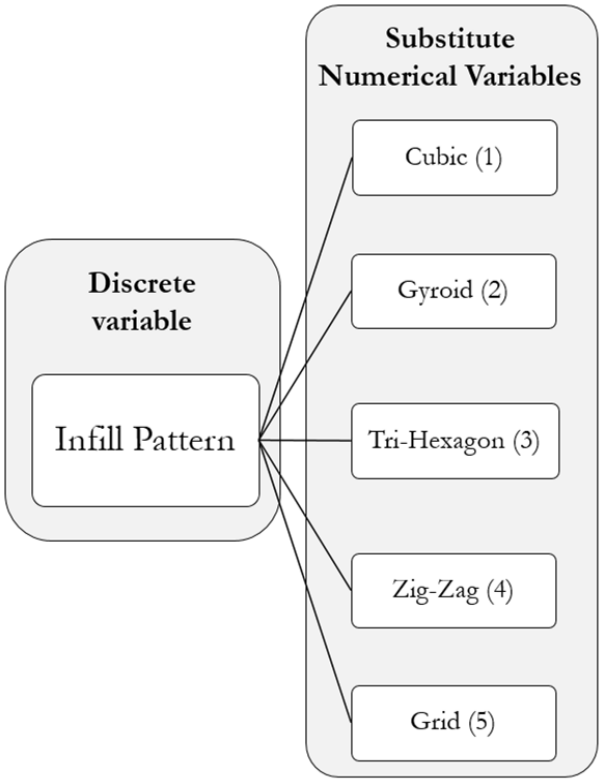

Fig. 7 *A scheme for decoding the categorical variable Infill Pattern into five numerical dummy variables which can only take the values 0 or 1*

Tab. 3 *Decoded numerical dummy variable values when analyzing each different infill pattern*

Infill pattern	Numerical dummy variables				
	infill_pattern_1	infill_pattern_2	infill_pattern_3	infill_pattern_4	infill_pattern_5
Cubic	1	0	0	0	0
Gyroid	0	1	0	0	0
Tri - Hexagon	0	0	1	0	0
Zig - Zag	0	0	0	1	0
Grid	0	0	0	0	1

4.2 Results and analysis for σ

The results shown in Fig. 8 summarize the impact of different infill patterns and densities on the ultimate tensile strength of the 3D-printed parts. Overall, the tensile strength increased with higher infill density across all patterns. At 25% infill, the ZigZag pattern yields the highest strength (16.40 MPa), while the TriHexagon pattern shows the lowest (12.76 MPa). At 50%, ZigZag and Gyroid patterns outperform the rest, reaching 19.52 MPa and 20.00 MPa respectively. At 75% infill, ZigZag maintains the highest strength (23.60 MPa), followed closely by Gyroid (22.50 MPa). It is important to note that the Grid and TriHexagon infills consistently show lower tensile strength across all densities.

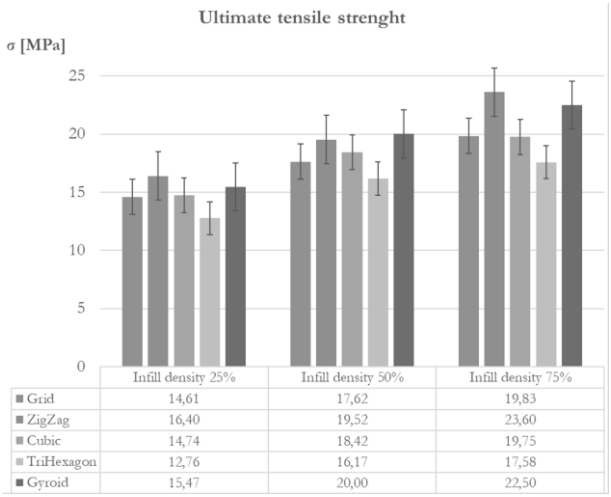

Fig. 8 *Bar chart that shows the stress (σ) distribution across all infill patterns and infill densities*

The individual value plot on Fig. 9 shows that as infill density increases, the sigma values (σ) also tend to increase for all infill patterns, indicating that higher infill densities generally result in stronger material properties. However, a pattern-dependent variation in σ does appear, which means that the choice of infill configuration does significantly affect material performance.

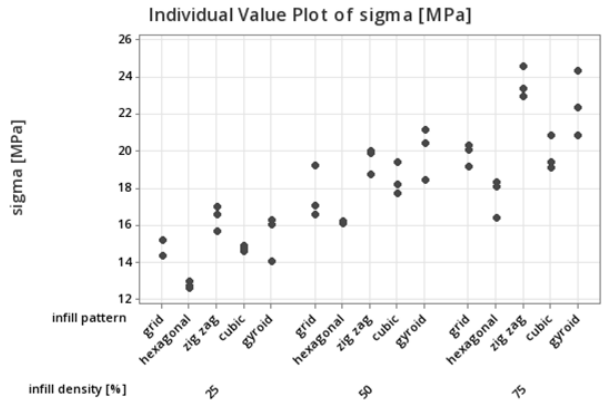

Fig. 9 *Individual Value Plot of σ [MPa]*

Among the five patterns, ZigZag and Gyroid are the most promising, because they exhibit the highest tensile strengths at all tested densities. Notably, at 75% infill, ZigZag and Gyroid reach the highest tensile strengths, approaching 24–25 MPa, with relatively low variation between replicates, indicating consistent performance. TriHexagon and Grid, on the other hand, register a lower average tensile strength. The data also reveal that while all patterns benefit from increased infill, the rate of strength improvement varies and some infill patterns show more substantial gains compared to others.

The main effects plot (Fig. 10) shows how infill density and infill pattern independently affect the mean ultimate tensile strength (σ). The left panel demonstrates a strong positive correlation between infill density and tensile strength, increasing the infill density from 25% to 75% results in a substantial increase in the mean tensile strength, rising from approximately 15 MPa to just over 20 MPa.

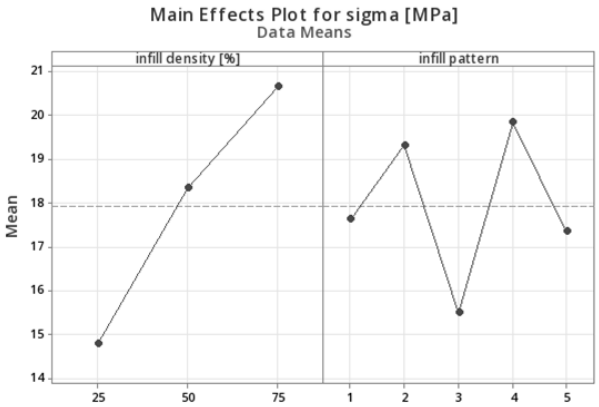

Fig. 10 *Main Effects Plot for σ [MPa]*

The right panel displays the mean effect of the different infill patterns, labeled 1 through 5 (corresponding to the pattern annotation in Fig. 5*)*. The mean tensile strength values of patterns 2 (Gyroid) and 4 (Zig - Zag) are highest, suggesting that they are most efficient in enhancing the structural performance. Pattern 3 (Tri - Hexagon) on the other hand, has the lowest average tensile strength implying that it might not be structurally efficient. While both factors influence strength, infill density has a more linear and pronounced effect, as was initially hypothesized.

On the interaction plot on Fig. 11, a consistent upward shift in mean strength is observed with increasing density, confirming that higher infill densities significantly enhance tensile performance.

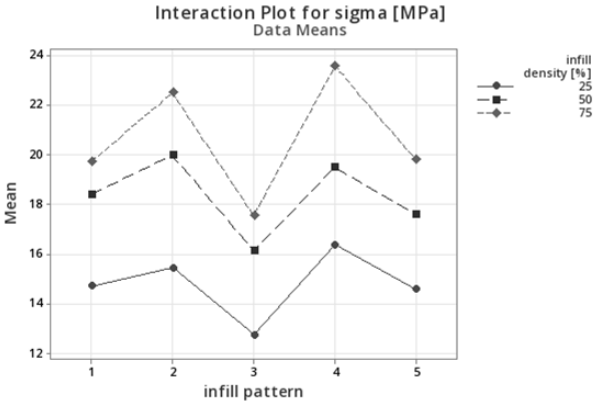

Fig. 11 *Interaction Plot for σ [MPa]*

However, the interaction between infill density and pattern is evident from the non-parallel lines: the relative performance of patterns changes across densities. At 75% density, patterns 2 (Gyroid) and 4 (ZigZag) exhibit peak strengths near 23–24 MPa,

whereas pattern 3 (TriHexagon) consistently underperforms at all densities. Notably, the spread between patterns is more pronounced at higher densities, suggesting that the choice of infill pattern becomes increasingly critical as density increases.

The mechanical trends observed across infill patterns and densities can be explained by considering how internal geometry governs load transfer, stress concentration, and failure initiation. At lower infill densities (25%), the load-bearing cross-section is sparse, which means that tensile forces are carried primarily by isolated filament roads. Under these conditions, patterns such as ZigZag and Gyroid perform better because their continuous, smoothly varying filament paths reduce abrupt directional changes and minimize stress concentrations. In contrast, patterns like Tri-Hexagon, Grid and Cubic contain more junctions and angular transitions, which promote localized stress accumulation and earlier crack initiation.

As density increases (50% and 75%), the effective load-bearing area grows, improving stiffness and strength by restricting deformation pathways. However, the internal geometry still plays a critical role. Patterns such as Gyroid and ZigZag retain mechanically efficient load paths even at high densities, enabling more uniform stress distribution and delaying the onset of micro-void coalescence or filament-interface debonding. Conversely, patterns with pronounced geometric discontinuities, such as Tri-Hexagon, develop localized brittle zones where filament intersections act as weak points. The result is the observed divergence in tensile strength and modulus between efficient and inefficient infill geometries at 75% density.

Tab. 4 *Regression coefficients for the ultimate tensile strength (σ) regression model*

Source	DF	Adj SS	Adj MS	F-Value	P-Value
infill density [%]	2	261.28	130.642	127.60	0.000
infill pattern	4	107.1	26.774	26.15	0.000
Error	28	38.91	1.024		
Lack-of-Fit	8	11.79	1.474	1.63	0.158
Pure Error	30	27.11	0.904		
Total	44	407.29			

The regression coefficients from the ANOVA for the regression model predicting ultimate tensile strength (σ) are shown in Tab. 4. The results indicate that both infill density and infill pattern are statistically significant factors influencing tensile performance. Infill density has the highest contribution to the model, with an adjusted sum of squares (Adj SS) of 261.28 and an F-value of 127.60, accompanied by a P-value of 0.000, which confirms its strong significance. Infill pattern also plays a significant role, with an Adj SS of 107.10 and an F-value of 26.15, also highly significant (P = 0.000). The error term (residual variation) is relatively low (Adj SS = 38.91), indicating a good model fit. Furthermore, the lack-of-fit test shows a P-value of 0.158, which is not significant, suggesting that the model does not suffer from systematic bias and adequately captures the variation in the data. The results from the ANOVA confirm that the chosen regression model is statistically valid and that both infill density and pattern significantly affect ultimate tensile strength, with infill density having the most dominant impact.

The results of the linear regression analysis showed the following predictive equation for Ultimate Tensile Strenght (σ, in MPa):

$$\sigma = 14.5 + 0 \cdot P_1 + 1.69 \cdot P_2 - 2.13 \cdot P_3 + 2.2 \cdot P_4 - 0.29 \cdot P_5 + 0 \cdot D[25\%] + 3.55 \cdot D[50\%] + 5.86 \cdot D[75\%] \quad (1)$$

Where:

σ…The ultimate tensile strength [MPa],

P_1 through P_5…The decoded discrete variables for the Infill Patterns (Fig. 5, Fig. 7),

D[25%], D[50%] and D[75%]…The infill densities.

Each coefficient represents the estimated effect of a specific infill pattern or density relative to a baseline category.

Tab. 5 *Model summary of the regression analysis for the ultimate tensile stress*

S	R-sq	R-sq(adj)	R-sq(pred)
1.04695	89.50%	88.16%	86.04%

The high coefficient of determination (R^2 = 89.5%) indicates that the model explains 89.5% of the variance in tensile strength, demonstrating strong predictive accuracy and confirming that infill pattern and density are major contributors to mechanical performance (Tab. 5). Increasing infill density from 25% to 50% and 75%, has a significant positive impact on the strength (σ) of the part, as shown by

the positive coefficients for all density levels. Different infill patterns influence σ differently. Patterns 2 (gyroid) and 4 (zig- zag) indicate a strengthening effect, while patterns 3 (trihexagon) and 5 (grid) suggest a weakening impact on tensile strength.

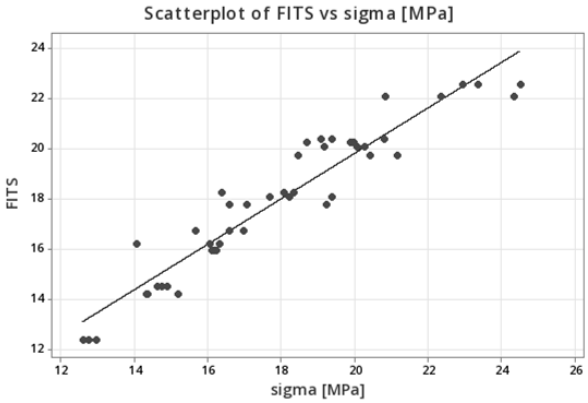

Fig. 12 *Scatterplot of FITS vs σ [MPa]*

The scatterplot of FITS (fitted values) versus actual tensile strength values (Fig. 12) shows a positive linear relationship. As σ increases, fitted values also tends to increase. The red trend line indicates that the data points generally follow a linear trend, suggesting that σ is a good predictor of fitted values within the observed range. The close clustering of most data points around this line shows that the model's predictions are highly accurate, with only minor deviations and no identified outliers.

4.3 Results and analysis for ε

The chart in Fig. 13 presents the relative strain at break for the various infill patterns across the three infill densities. At all densities, Grid, Gyroid and ZigZag patterns consistently achieve higher strain values, indicating better ductility. Specifically, at 25% infill, ZigZag exhibits the highest strain (3.10%), followed closely by Gyroid (2.98%) and Grid (2.82%), while TriHexagon records the lowest (2.50%). This trend continues at 50% infill, where Grid achieves the highest strain (3.48%), and again TriHexagon the lowest (2.87%). At 75% infill, Grid, ZigZag and Gyriod maintain the highest values (3.47%, 3.32% and 3.30%, respectively), while TriHexagon and Cubic remain lower (2.56% and 2.65%). These results indicate that Grid, ZigZag, and Gyroid infill patterns are more favorable for applications requiring greater deformation before failure, as they consistently offer higher relative strain at break values compared to Cubic and TriHexagon.

The individual value plot for relative strain at break (ε) in Fig. 14 shows the distribution of strain values across the various infill patterns and densities. Unlike tensile strength, relative strain does not exhibit a consistent trend with increasing infill density. At 25% infill, strain values are relatively lower, with limited variation across patterns. At 50% infill, there is slightly greater dispersion, with several data points reaching higher strain values, suggesting improved ductility for certain infill configurations.

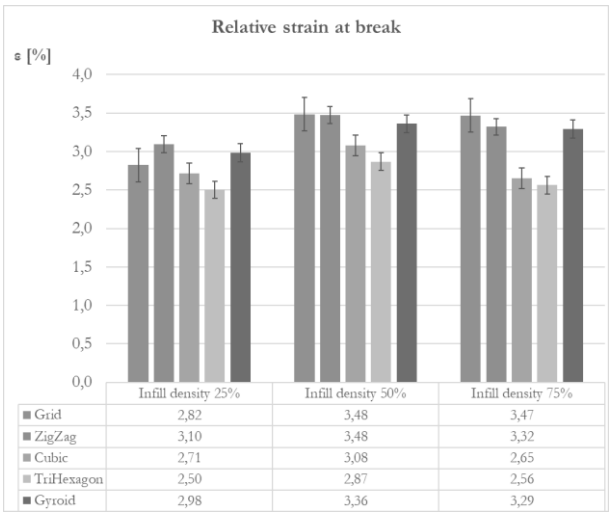

Fig. 13 *Bar chart that shows the strain (ε) distribution across all infill patterns and infill densities*

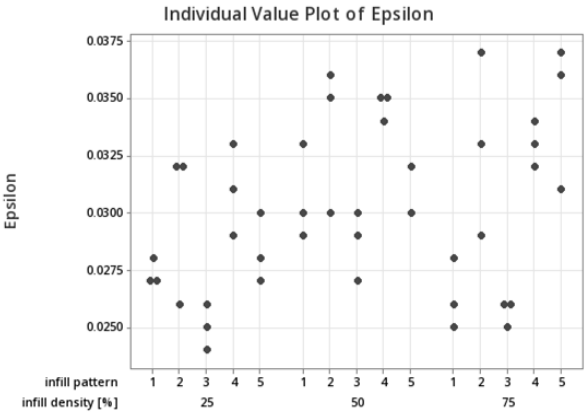

Fig. 14 *Individual Value Plot of ε [-]*

Interestingly, at 75% infill density, many strain values appear lower or comparable to those at 25%, particularly for patterns 1 (Cubic) and 4 (Zig-Zag), indicating a potential loss in ductility at higher densities. In contrast, patterns 2 (Gyroid) and 5 (Grid) maintain higher strain values across all densities, highlighting their capacity to retain flexibility even at higher stiffness levels.

The main effects plot for relative strain at break (ε), representing mean relative strain at break, shows how infill density and infill pattern influence ductility (Fig. 15). In the left panel, the strain increases from 25% to 50% infill density, peaking at 50%, then slightly declines at 75%. This suggests that moderate infill density may optimize ductility, while higher densities may constrain deformation due to increased structural rigidity.

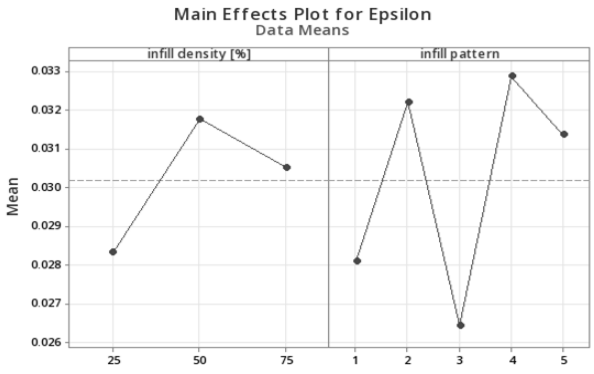

Fig. 15 *Main Effects Plot for ε [-]*

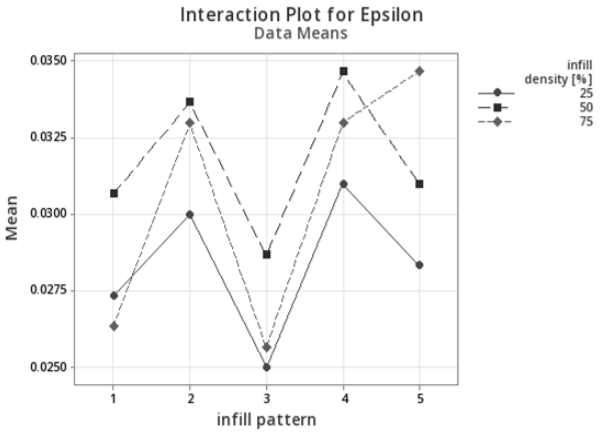

Fig. 16 *Interaction plot for ε [-]*

In the right panel, the infill pattern has a more pronounced effect on strain. Pattern 4 (Zig-Zag) shows the highest mean strain, followed by pattern 5 (Grid), indicating superior ductility. In contrast, pattern 3 (Tri-Hexagon) exhibits the lowest mean strain, suggesting it is the most brittle among the group. Patterns 1 (Cubic) and 2 (Gyroid) fall in the middle range. These trends reinforce that while infill density affects strain, the choice of infill pattern is a stronger determinant of deformation behavior, with patterns Zig-Zag and Grid being most suitable for applications where flexibility and energy absorption is important.

The interaction plot for for ε (Fig. 16), with no parallel lines, indicates a clear interaction between the two factors. At 50% infill density, all patterns show a general increase in strain, with patterns 2 (Gyroid) and 4 (Zig-Zag) reaching the highest values. Pattern 3 (Tri-Hexagon) consistently demonstrates the lowest strain across all densities, indicating poor deformation capacity regardless of density.

Interestingly, the plot shows that while pattern 4 (Zig-Zag) benefits most from increased infill density, peaking at 75%, other patterns such as 2 (Gyroid) and 5 (Grid) maintain relatively high strain at both 50% and 75%, suggesting they are less sensitive to density changes in terms of ductility. Pattern 1 (Cubic) exhibits a steady but moderate strain performance, while pattern 3 (Tri-Hexagon) again remains the least ductile across the board.

The strain behavior also reflects the mechanisms that govern the stress distribution of the specimens described previously. Maximum strain occurs where the internal geometry permits controlled deformation prior to failure. Grid, ZigZag and Gyroid infills, having more continuous paths along the loading axis, allow limited redistribution of stress, which enhances ductility. Meanwhile, patterns with more rigid, closed-cell shapes such as Tri-Hexagon restrict deformation, leading to premature fracture and lower strain values.

Tab. 6 *Regression coefficients for the relative strain (ε) regression model*

Source	DF	Adj SS	Adj MS	F-Value	P-Value
infill density [%]	2	0.000128	0.000064	9.18	0.001
infill pattern	4	0.000315	0.000079	11.28	0.000
Error	38	0.000265	0.000007		
Lack-of-Fit	8	0.000049	0.000006	0.84	0.572
Pure Error	30	0.000217	0.000007		
Total	44	0.000709			

The ANOVA table for the regression model predicting relative strain at break (ε) (Tab. 6) demonstrates that both infill density and infill pattern have statistically significant effects on strain behavior. The infill pattern shows a slightly greater influence, with an F-value of 11.28 and a highly significant P-value of 0.000, indicating that the geometry of the internal structure significantly affects ductility. Infill density is also significant, with an F-value of 9.18 and P = 0.001, suggesting that changes in density meaningfully influence how much the material can elongate before failure. The model's error variance is small (Adj SS = 0.000265), and the lack-of-fit test yields a P-value of 0.572, indicating no significant lack of fit which validates the model's adequacy. The results from the analysis confirm that the model effectively captures the variability in strain behavior of FDM-printed parts and that both infill parameters are important predictors of ε, with the infill pattern type having a slightly stronger impact.

The results of the linear regression analysis showed the following predictive equation for the maximum relative strain at break (ε, in %):

$$\varepsilon = 2.62 + 0 \cdot P_1 + 0.41 \cdot P_2 - 0.17 \cdot P_3 + 0.48 \cdot P_4 + 0.35 \cdot P_5 + 0 \cdot D[25\%] + 0.35 \cdot D[50\%] + 0.22 \cdot D[75\%] \quad (2)$$

Where:

ε…The relative strain at break [%],

P_1 through P_5…The decoded discrete variables for the Infill Patterns (Fig. 5, Fig. 7),

D[25%], D[50%] and D[75%]…The infill densities.

Pattern 4 (Zig-Zag) and 5 (Grid) have a positive effect, enhancing ductility, while pattern 3 (Tri-Hexagon) slightly reduces it. The pattern 2 (Gyroid) also has a positive effect, but its influence on the strain is negligible. Among the densities, the highest contribution comes from D[50%], suggesting that moderate density supports greater strain, whereas D[75%] shows a smaller positive effect.

Tab. 7 *Model summary of the regression analysis for the relative strain at break*

S	R-sq	R-sq(adj)	R-sq(pred)
0.0023263	65.03%	59.36%	50.37%

Overall, this model highlights the relatively small but measurable influence of infill parameters on strain behavior. The model's coefficient of determination (R^2 = 65.03%) indicates a moderate level of explanatory power, meaning the equation accounts for about 65% of the variation in strain values (Tab. 7). This suggests that while infill pattern and density significantly influence ductility, other factors may also contribute to the variability observed in the experimental results.

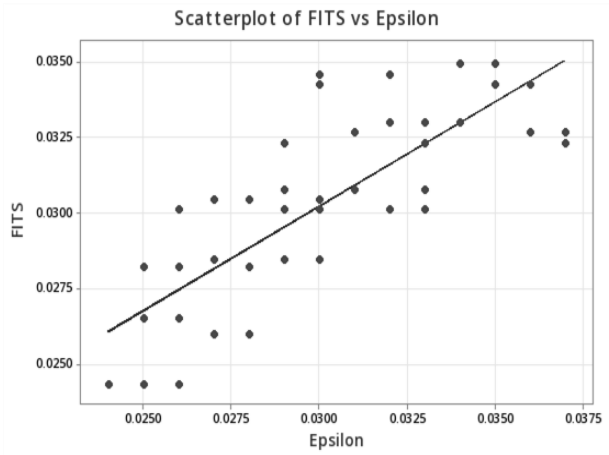

Fig. 17 *Scatterplot of FITS vs ε*

On the scatterplot of FITS versus ε (Fig. 17) most data points align closely along the trend line, though some scatter is evident, particularly in the midrange, indicating modest prediction variability. This visual pattern aligns with the model's coefficient of determination (R^2 = 65.03%), which reflects a moderate level of predictive accuracy. Overall, the plot confirms that the model captures the general trend of the data but leaves room for improvement in predicting strain behavior with precision.

4.4 Results and analysis for E

The chart in Fig. 18 illustrates the elastic modulus of the 3D-printed specimens with different infill patterns and densities, revealing a clear trend of increasing stiffness with higher infill density. At 25% infill, all patterns exhibit relatively similar moduli, with values ranging from approximately 510 MPa to 543 MPa. At 50% infill, elastic modulus increases slightly across all patterns, with Cubic and Gyroid (598.32 MPa and 596.03 MPa, respectively) showing the highest values. At 75% infill, the differences become more pronounced. Cubic reaches the highest stiffness (745.08 MPa), followed by ZigZag (709 MPa), while Grid (574.76 MPa) remains lower.

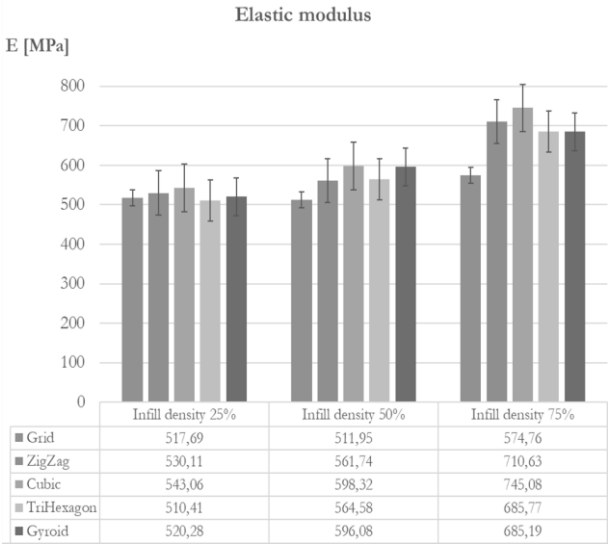

Fig. 18 *Bar chart that shows the elastic modulus (E) distribution across all infill patterns and infill densities*

As expected, the individual value plot (Fig. 19) for the elastic modulus (E) shows how that increasing infill density from 25% to 75% leads to a clear upward shift in elastic modulus, indicating greater rigidity with denser internal structures.

At 25% infill density, most values are concentrated between 500 and 550 MPa with relatively low variation, indicating that at low density, the choice of infill pattern has minimal impact on stiffness. At 50% density, there is a modest increase in modulus for some patterns (particularly pattern 5 - Grid), but the spread remains fairly tight, suggesting moderate influence of geometry at this level.

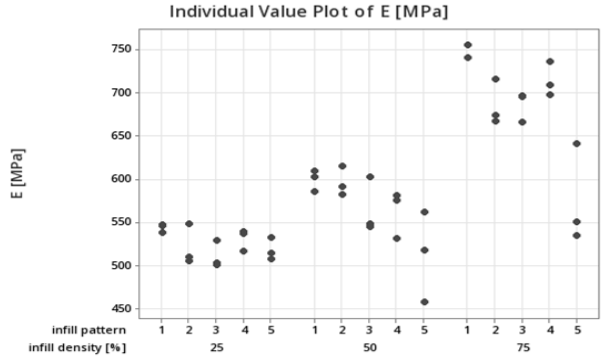

Fig. 19 *Individual Value plot of E [MPa]*

The most significant increase in elastic modulus occurs at 75% infill density, where several values exceed 700 MPa. Patterns 1 (Cubic), 3 (Tri–Hexagon), and 4 (Zig–Zag) at this density show the highest stiffness values, while pattern 5 (Grid) presents more moderate values. This sharp rise and greater spread at high density underscore the strong interaction between infill density and pattern, suggesting that structural rigidity is maximized when both parameters are optimized. The plot confirms that infill density is the dominant factor influencing stiffness, with the effect of infill pattern becoming increasingly important at higher densities.

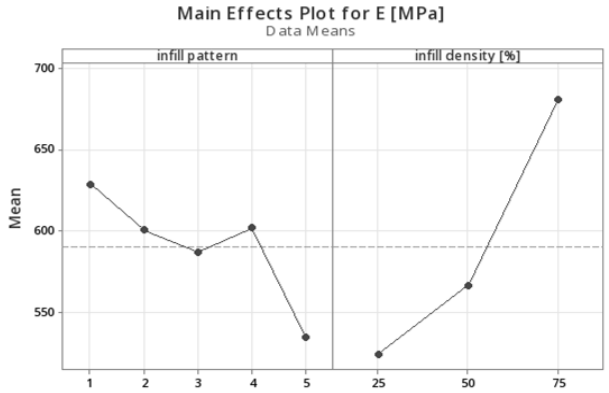

Fig. 20 *Main Effects Plot of E [MPa]*

In the left panel of the main effects plot (Fig. 20), the mean elastic modulus varies across infill patterns. Pattern 1 (Cubic) yields the highest mean stiffness, followed by patterns 2 (Gyroid) and 4 (Zig-Zag), while pattern 5 (Grid) shows a noticeable drop, indicating it provides the least stiffness on average among the five patterns evaluated.

In the right panel, the effect of infill density is strongly pronounced. The mean elastic modulus increases significantly from 25% to 75% infill, with a clear, nearly linear upward trend. This confirms that increasing infill density directly enhances stiffness, with 75% infill producing the highest average elastic modulus (near 700 MPa), while 25% infill results in the lowest (around 530 MPa).

The interaction plot for the elastic modulus (E) reveals how the relationship between infill pattern and infill density affects the stiffness of 3D-printed materials (Fig. 21). The three lines represent 25%, 50%, and 75% infill densities, with clear separation indicating that infill density is a dominant factor in determining stiffness.

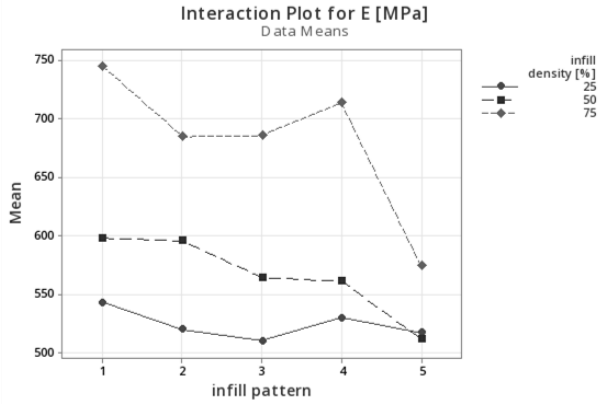

Fig. 21 *Interaction Plot for E [MPa]*

At 25% and 50% densities, the elastic modulus remains relatively low and consistent across all infill patterns, showing only minor variations. However, at 75% infill, differences between patterns become more pronounced. Pattern 1 (Cubic) yields the highest modulus, while pattern 5 (Grid) shows the lowest among the group at this density. The descending slope of the green line (75%) suggests that the stiffness advantage conferred by higher infill density is most sensitive to the choice of pattern.

The non-parallel nature of the lines indicates interaction effects: the performance of each infill pattern changes in magnitude and rank depending on the infill density.

Tab. 8 *Regression coefficients for the Young elastic modulus (E) regression model*

Source	DF	Adj SS	Adj MS	F-Value	P-Value
infill density [%]	2	197179	98589.7	83.93	0.000
infill pattern	4	43451	10862.7	9.25	0.000
Error	38	44639	1174.7		
Lack-of-Fit	8	22712	2839.0	3.88	0.003
Pure Error	30	21927	730.9		
Total	44	285269			

The regression coefficients from the ANOVA for the regression model predicting the Young's modulus (E) are shown in Tab. 8. The values reveal that both infill density and infill pattern significantly affect the elastic behavior of FDM-printed parts. Infill density is the dominant factor, with an adjusted sum of squares (Adj SS) of 197,179 and an F-value of 83.93, accompanied by a P-value of 0.000, confirming there is a strong statistical significance. Infill pattern also meaningfully contributes, with an Adj SS of 43,451, an F-value of 9.25, and a P-value of 0.000, indicating that the internal geometry also plays a crucial role in determining stiffness. The model's residual error is relatively moderate (Adj SS = 44,639), but the lack-of-fit test is significant (P = 0.003), suggesting that the model may not fully capture all sources of variation in the data. Despite this, the high F-values and significant P-values indicate that the model effectively identifies the primary variables influencing Young's modulus, with infill density exerting the most pronounced effect.

The results of the linear regression analysis showed the following predictive equation for the Elastic modulus (E, in MPa):

$$E = 562.5 + 0 \cdot P_1 - 28.3 \cdot P_2 - 41.9 \cdot P_3 - 26.9 \cdot P_4 - 94.1 \cdot P_5 + 0 \cdot D[25\%] + 42.3 \cdot D[50\%] + 156.7 \cdot D[75\%] \quad (3)$$

The regression equation models the elastic modulus (E) as a function of infill pattern, P_1 through P_5 (Fig. 5, Fig. 7), and infill density (D[25%], D[50%], D[75%]). The baseline value is 562.5 MPa, with pattern 1 (Cubic) as the reference. Patterns 2 through 5 contribute negatively to stiffness, with pattern 5 (Grid) having the most substantial reduction (–94.1 MPa), indicating it results in significantly lower modulus compared to the reference. In contrast, the infill density terms show a strong positive influence: increasing from 25% to 75% boosts the modulus by as much as 156.7 MPa. The model's coefficient of determination (R^2 = 84.35%) suggests high predictive power in explaining the variability in stiffness (Tab. 9).

Tab. 9 *Model summary of the regression analysis for the module of elasticity E*

S	R-sq	R-sq(adj)	R-sq(pred)
34.2741	84.35%	81.88%	78.06%

The scatterplot (Fig. 22) evaluates the accuracy of the regression model. Most data points conform to the trend line, particularly in the higher modulus range (above 600 MPa), indicating strong predictive alignment in that region. Some dispersion is visible in the mid and lower modulus ranges, suggesting slightly less precision in those areas. Overall, the plot supports the model's coefficient of determination (R^2 = 84.35%), confirming that the model follows the key trends and provides reliable predictions of stiffness.

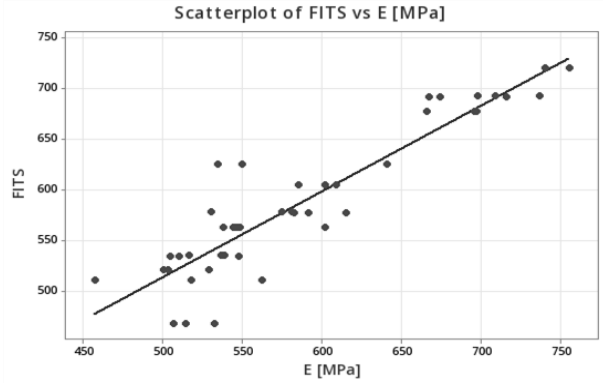

Fig. 22 *Scatterplot of FITS vs E [MPa]*

5 Discussion

This study systematically examined the mechanical behavior of PLA specimens produced using FDM, focusing on the effects of infill pattern and infill density on tensile strength, relative strain at break, and elastic modulus. The results reinforce widely reported trends in the literature, while also clarifying the mechanical principles underlying the observed behaviors.

Consistent with previous findings by Karad et al. [5] and Garg et al. [11], infill density emerged as the dominant factor influencing mechanical performance. Increasing density from 25% to 75% produced significant gains in tensile strength and stiffness, as confirmed by high F-values and strong statistical significance in the ANOVA results. This behavior is expected, as higher infill density reduces internal porosity and increases the load-bearing cross section, enabling better transmission of stresses through the printed structure. The regression models developed in this study further demonstrate the strength of this relationship, with infill density showing the largest positive coefficients for both σ and E.

The influence of infill pattern observed here aligns closely with existing literature on FDM structural mechanics. Gyroid and ZigZag infills exhibited superior mechanical performance across all densities, confirming observations by Kadhum et al. [7]. Gyroid structures offer smooth, continuous curvature without sharp inter-filament intersections, promoting uniform stress distribution and reducing stress concentration points. ZigZag infill benefits from long, continuous raster paths aligned with the tensile loading direction, improving load transfer and delaying fracture initiation. These geometric characteristics translate directly to the higher tensile strength and ductility observed in this study.

In contrast, patterns such as Tri-Hexagon and Grid consistently underperformed, an outcome supported by Agrawal et al. [3], who note that geometries with frequent angular intersections tend to accumulate localized stresses, while continuous curvature patterns improved tensile strength and impact strength due to the interruption of crack propagation and better stress distribution. In the present study, the Tri-Hexagon pattern yielded the lowest tensile strengths and lowest strain values across most test cases. The mechanical explanation is that sharp geometric features and repeated junctions act as stress-riser sites where micro-cracks can nucleate more easily under tension, causing early brittle failure. This behavior was most apparent at 75% infill density, where geometric complexity amplified internal constraints and limited deformation.

The strain-at-break results additionally support the relationship between geometry and deformation behavior. Grid and ZigZag infills, which provide more open and continuous deformation pathways, produced higher strain values. Meanwhile, the more constrained Tri-Hexagon and Cubic geometries restricted strain, leading to more brittle fracture modes. Also, the decreased elongation in specimens with higher density in this study matches the behavior reported by Daly et al. [10], who found that FDM patterns with limited deformation pathways tend to exhibit early crack propagation and a prominent unit structure would typically permit more rotation space and flexibility along the axial extension direction, resulting in a higher elongation at lower infill percentages.

From a mechanical interpretation standpoint, the performance differences between infill patterns can be explained by their internal load-flow architectures. Efficient patterns such as Gyroid and ZigZag behave analogously to optimized cellular or truss structures, where stresses are transferred through continuous and smoothly varying paths. These structures reduce the likelihood of shear localization and interlayer debonding. Inefficient geometries, such as Tri-Hexagon, impose abrupt directional changes that create internal constraints and promote localized stress buildup. As a result, stress cannot be uniformly redistributed, so failure initiates earlier and propagates rapidly.

The elastic modulus results further reflect this interplay between geometry and mechanical efficiency. At higher densities, Cubic, ZigZag and Gyroid infills exhibited the highest stiffness values, consistent with reports by Birosz and Ando [6] that geometrically continuous infills enhance rigidity. Grid, despite its simple orthogonal architecture, showed lower stiffness due to filament junctions that allow shear displacement under axial loading. The increasing separation between patterns at 75% infill suggests that geometric effects become amplified as the internal structure becomes more constrained.

Overall, the findings of this research corroborate established trends and contribute new quantitative evidence regarding the mechanical impact of commonly used infill strategies. By integrating statistical modeling, mechanical reasoning, and comparisons with existing literature, this study demonstrates how specific geometric features govern stress distribution, deformation behavior, and structural robustness in FDM-printed PLA components. These insights are valuable for practitioners seeking to optimize print parameters for strength-critical applications and highlight the need to consider infill geometry as a fundamental structural design variable in additive manufacturing.

5.1 Limitations, sources of inaccuracy and future work

While this research is a thorough investigation of the mechanical effect of infill pattern and infill density and there are a couple of opportunities that can be used in the future research. Further tests may explore how the printing parameters, including layer height, print orientation, and nozzle temperature, affect mechanical performance and how such advanced and hybrid infill patterns [15], including honeycomb, Hilbert curve, and Voronoi, can improve it. Additionally, the use of more advanced or a combination of materials, like carbon-fiber-reinforced or glass-filled PLA, would clarify the connection between material reinforcement and internal geometry [13]. Fatigue testing and dynamic loading conditions would expand this understanding beyond static tensile behavior, making the results more applicable to real-world use cases.

Although the experimental design and statistical modeling in this study provide meaningful insights into the mechanical effects of infill pattern and density, several limitations must be acknowledged. First, the PLA filament was not actively dried prior to printing, despite its hygroscopic nature. Variations in moisture content may have introduced inconsistencies in extrusion quality, interlayer adhesion, and overall mechanical performance. This factor represents an uncontrolled source of material variability that may influence tensile strength, strain at break, and elastic modulus.

Print orientation is another parameter that was held constant but is known to be a major contributor to anisotropic mechanical behavior in FDM. Since all specimens were printed in the same X–Y plane orientation, the study effectively captures only the mechanical response associated with this specific layering arrangement. Tensile loading parallel to filament deposition paths typically yields higher strength and ductility, whereas loading perpendicular

to layer interfaces often results in brittle failure or delamination. Therefore, while the results accurately reflect the effect of infill pattern and density under this orientation, they cannot be generalized across all printing directions. Incorporating multiple build orientations in future research would enable a more comprehensive assessment of how anisotropy interacts with internal infill geometry and density

Although printing parameters such as nozzle temperature, layer height, print speed, and wall thickness were held constant, minor fluctuations in ambient laboratory conditions (temperature, humidity, airflow) and machine-specific behaviors (extruder pressure stability, micro-vibrations, and mechanical tolerances) could have contributed to small variations among specimens.

Additionally, geometric deviations caused by slicer discretization or by machine inaccuracies, such as filament deposition width inconsistency, slight warping at specimen ends, or microscopic voids between rasters, may influence measured properties. Such imperfections, while typical in FDM manufacturing, introduce uncertainties not explicitly quantified in this study.

Finally, the regression models, while statistically strong, rely on linear approximations and dummy-variable encoding that simplify the complex nonlinear behavior of polymer extrusion and fracture. The significant lack-of-fit detected in the elastic modulus model indicates that additional nonlinear terms or interaction effects may exist but were not captured.

Together, these limitations frame the context of the results and highlight areas where tighter process control or expanded experimental design would improve accuracy and generalizability.

References

[1] J. LIU et al., Effect of Infill Parameters on the Compressive Strength of 3D-Printed Nylon-Based Material, *Polymers* (Basel)., vol. 15, no. 2, p. 255, Jan. 2023, doi: 10.3390/polym15020255.

[2] S. PATIL, T. SATHISH, J. GIRI, B. F. FELEMBAN, An experimental study of the impact of vari-ous infill parameters on the compressive strength of 3D printed PETG/CF, *AIP Adv.*, vol. 14, no. 9, Sep. 2024, doi: 10.1063/5.0212544.

[3] A. P. AGRAWAL, V. KUMAR, J. KUMAR, P. PARAMASIVAM, S. DHANASEKARAN, L. PRASAD, An investigation of combined effect of infill pattern, density, and layer thickness on mechanical properties of 3D printed ABS by fused filament fabrication, *Heliyon*, vol. 9, no. 6, p. e16531, Jun. 2023, doi: 10.1016/j.heliyon.2023.e16531.

[4] M. RISMALIA, S. C. HIDAJAT, I. G. R. PERMANA, B. HADISUJOTO, M. MUSLIMIN, F. TRIAWAN, Infill pattern and density effects on the tensile properties of 3D printed PLA material, *J. Phys. Conf. Ser.*, vol. 1402, no. 4, p. 044041, Dec. 2019, doi: 10.1088/1742-6596/1402/4/044041.

[5] J. PERNICA, M. SUSTR, P. DOSTAL, M. BRABEC, D. DOBROCKY, Tensile Testing of 3D Printed Materials Made by Different Temperature, *Manufacturing Technology*, vol. 21, no. 3, pp. 398–404, Jun. 2021, doi: 10.21062/mft.2021.039.

[6] A. S. KARAD, P. D. SONAWWANAY, M. NAIK, D. G. THAKUR, Experimental study of effect of infill density on tensile and flexural strength of 3D printed parts, *Journal of Engineering and Applied Science*, vol. 70, no. 1, p. 104, Dec. 2023, doi: 10.1186/s44147-023-00273-x.

[7] M. T. BIROSZ, M. ANDÓ, Effect of infill pattern scaling on mechanical properties of FDM-printed PLA specimens, *Progress in Additive Manufacturing*, vol. 9, no. 4, pp. 875–883, Aug. 2024, doi: 10.1007/s40964-023-00487-8.

[8] A. H. KADHUM, S. AL-ZUBAIDI, S. S. ABDULKAREEM, Effect of the Infill Patterns on the Me-chanical and Surface Characteristics of 3D Printing of PLA, PLA+ and PETG Materials, *ChemEngineering*, vol. 7, no. 3, p. 46, May 2023, doi: 10.3390/chemengineering7030046.

[9] A. FALES, V. ČERNOHLÁVEK, M. SUSZYNSKI, J. ŠTĚRBA, P. BALCAR, P. HOUŠKA, 3D Printing - Weight Optimization of FDM-Printed Components Using PLA and PETG, *Manufacturing Technology*, Apr. 2026, doi: 10.21062/mft.2026.026.

[10] A. FALES, V. ČERNOHLÁVEK, M. SUSZYNSKI, J. ŠTĚRBA, P. BALCAR, P. HOUŠKA, 3D Printing - Dimensional Accuracy and Stability of PLA and PETG Prints Using the FDM Technology, *Manufacturing Technology*, vol. 26, no. 2, pp. 148–163, Apr. 2026, doi: 10.21062/mft.2026.020.

[11] Z. JOSKA, L. ANDRÉS, T. DRAŽAN, K. MAŇAS, Z. POKORNÝ, J. SEDLÁK, Influence of the shape of the filling on the mechanical properties of samples made by 3D printing, *Manufacturing Technology*, vol. 21, no. 2,

pp. 200–206, Apr. 2021, doi: 10.21062/mft.2021.024.

[12] "*EN ISO 527-2* Plastics - Test conditions for moulding and extrusion plastics."

[13] M. DALY, M. TARFAOUI, M. BOUALI, A. BENDARMA, Effects of Infill Density and Pattern on the Tensile Mechanical Behavior of 3D-Printed Glycolyzed Polyethylene Terephthalate Rein-forced with Carbon-Fiber Composites by the FDM Process, *Journal of Composites Science*, vol. 8, no. 4, p. 115, Mar. 2024, doi: 10.3390/jcs8040115.

[14] S. GARG, A. SARDAR, R. SRIVASTAVA, S. VERMA, A. K. MADAN, Variation in Tensile Strength of 3D Printed PLA Parts by Varying Infill Density and Infill Pattern, *Saudi Journal of Engineering and Technology*, vol. 8, no. 05, pp. 103–107, May 2023, doi: 10.36348/sjet.2023.v08i05.004.

[15] M. HAMOUD, O. M. MOMAMED, A. F. BARAKAT, A. SOBHI, Effect of new combined infill patterns and building strategy on the properties of FDM printed PLA parts, *Trends in ad-vanced sciences and technology*, vol. 1, no. 1, Jan. 2024, doi: 10.62537/2974-444X.1018.